IOP Conf. Series: Journal of Physics: Conf. Series **796** (2017) 012037 doi:10.1088/1742-6596/796/1/012037

Critical heat flux in a multi-minichannel heat sink. Effect of the heated length-on-diameter ratio

R MASTRULLO[1], A W MAURO[1,2] and L VISCITO[1]

[1]Department of Industrial Engineering, Federico II University of Naples, P.le Tecchio 80, 80125, Naples (Italy)

[2]e-mail: alfonsowilliam.mauro@unina.it

Abstract. This paper exhibits saturated CHF experimental values obtained with R134a and R1234yf, working at saturation temperatures from 25 °C up to 65 °C (i.e. reduced pressures from 0.16, 0.20 and up to 0.46, 0.54, respectively). The mass flux was let to vary from 150 up to 350 kg/m^2 s. All tests were performed with an aluminum multi-minichannel heat sink, made up of seven rectangular ducts, each of them 2 mm wide, 1 mm high and 35 mm long. Two heated lengths of 25 and 35 mm were structured, in order to study two different L_h/D_{eq} ratios. The results show that critical heat flux is enhanced with increasing the mass flux and decreasing the saturation temperature. A greater L_h/D_{eq} ratio leads instead to lower CHF values.

1. Introduction

The ongoing progresses in technology have made possible the use of densely packed integrated circuits (ICs) [1]-[2], laser mirrors and concentrated solar cells [3]. For the correct functioning of these devices, the heat must be dissipated within very small areas, thus leading to the necessity of removing high heat fluxes that exceed the air and the liquid forced convection cooling power.

Two-phase heat exchange devices represent valuable resources to replace the single-phase cooling methods. Microchannels and minichannels, by exploiting the boiling mechanism of synthetic refrigerants, are well suited for this task and provide large heat transfer surface area per unit length [4].

The operative limit of such system is represented by the critical heat flux (CHF), referring to the situation in which the heated wall loses contact with the liquid phase, yielding to a sudden drop of the heat transfer coefficient and therefore a sharp rise of the wall temperature, which may exceed the melting point of the channel material [5]. The capability to determine CHF is therefore of great importance, since a heat sink should be designed with a considerable amount of safety relative to the maximum heat flux dissipation that can be handled or the minimum refrigerant flow rate.

Different geometries, fluids and operating conditions have already been presented in scientific literature [6], although still limited sources cope with new low-GWP refrigerants at medium-to-high saturation temperatures. Furthermore, most of the studies are related to single channel geometries [7]; even if the basic CHF phenomenon in rectangular minichannels could be similar to that in round tubes, the existence of non-heated walls and possible mal-distribution [8] may lead to significant discrepancies among the experimental results available in literature. It is also known that the CHF is related to the channels heated length L_h and its impact has been usually measured with the use of the heated length over the equivalent diameter of the channel L_h/D as dimensionless parameter. Generally,

Content from this work may be used under the terms of the Creative Commons Attribution 3.0 licence. Any further distribution of this work must maintain attribution to the author(s) and the title of the work, journal citation and DOI.
Published under licence by IOP Publishing Ltd

CHF decreases with increasing L_h/D and some researchers [9]-[10] have reported threshold values of L_h/D beyond those it does not affect the critical condition anymore.

Wojtan et al. [11] investigated different conditions of boiling R134a and R245fa to obtain the saturated critical heat flux in 0.5 and 0.8 mm internal diameter tubes with two different heated lengths. They found that with the extension of the heated length from 20 to 70 mm, the drop of the CHF value was very intense (up to 40 W/cm^2).

Tanaka et al. [7] collected existing data and developed a CHF correlation for thin rectangular channels applicable to a wide range of heated lengths. The authors found that CHF was highly affected by the L_h/D parameter, especially for low mass flux condition, in which CHF dropped more than 350% passing from L_h/D = 50 to 179.

Wu and Li [10] also took experimental CHF values from existing databases, observing that CHF greatly decreased with L_h/D, for small values of the heated length. At a threshold of L_h/D = 150, it presented a negligible effect on the saturated CHF.

In this paper, some experimental saturated CHF results are presented in an aluminum multi-minichannel heat sink for two different working fluids, R134a and its low-GWP substitute R1234yf. With the same equivalent diameter for each channel of 1.33 mm, two different test section set ups have been arranged in order to achieve different heated lengths of 25 and 35 mm. The resulting L_h/D ratio is then 18.75 and 26.25, respectively, and its effect is analyzed in the form of diagrams and boiling curves. All tests present a saturation temperature range of 25-65 °C and a mass velocity range of 150-350 kg/m^2 s.

2. Experimental test rig and measurements uncertainties

The test facility has been assembled in the Refrigeration Laboratory, at the Industrial Engineering Department, Università degli Studi di Napoli Federico II. The whole set-up is made up of two different closed loops. In the main refrigerant loop, the working fluid conditions in terms of test section inlet saturation temperatures, sub-cooling and mass flow rate, are set and monitored. The latter is a water closed loop which is thermally controlled by a thermostatic bath. A schematic of the entire test rig is displayed in Fig. 1.

2.1. Refrigerant loop and water loop description

The main loop is the black line depicted in Fig. 1. The working fluid flows is driven by means of a magnetic gear pump through a Coriolis mass flow meter up to the test section, in which a Pt100 resistance thermometer and a piezoelectric pressure transducer measure the inlet thermodynamic conditions. The pressure drop across the test section is measured with a differential pressure transducer and another Pt100 resistance thermometer is placed at the outlet section. A manually-controlled throttling valve is employed in order to adjust the system pressure and the mass flow rate during the experiments. The refrigerant in two-phase conditions is condensed with a plate heat exchanger and then flows into a liquid receiver. The working fluid is finally sub-cooled by means of a double pipe heat exchanger before the pump suction head which closes the loop.

The magnetic gear pump may elaborate volumetric flow rates within a range of 1.3-2.5 dm^3/min, changing its rotating speed via inverter from 1650 rpm to 3400 rpm. In order to achieve very low mass flow rates flowing into the test section, the refrigerant loop is equipped with a by-pass circuit, manually controlled, which is able to recirculate the refrigerant surplus directly into the liquid receiver.

The secondary loop provides demineralized water to the sub-cooler and the condenser. Both the double pipe and the plate heat exchangers may be excluded from the water flow by employing two ball-cock valves. The desired water temperature is obtained with a remote-controlled external thermostatic bath. The secondary fluid specific volume variations are restricted thanks to an expansion vessel.

Both the main and the secondary loop are provided with several Pt100 resistance thermometers to monitor the thermodynamic conditions in the entire test rig (see Fig. 1).

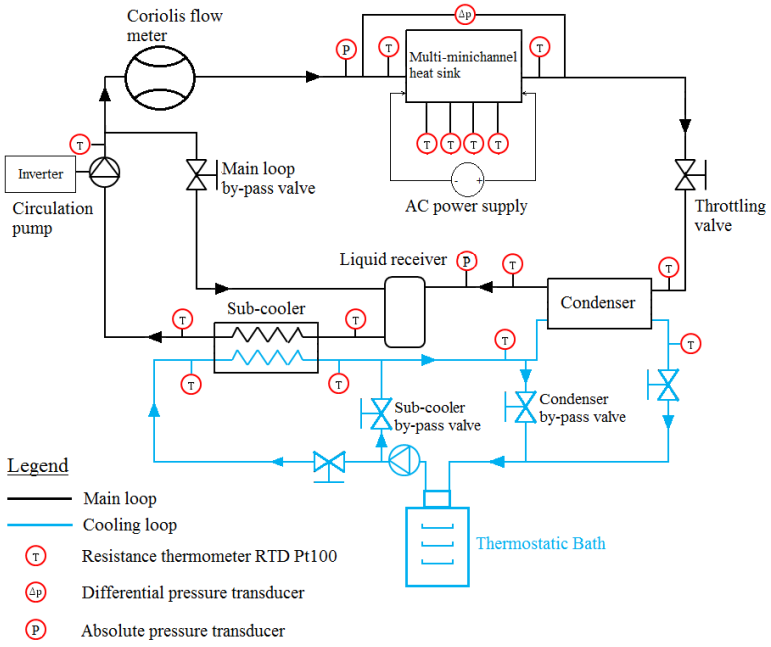


Figure 1. Sketch of the test facility

2.2. Test section

The test section used for all the experiments presented in this paper consists of an aluminum multi-minichannel heat sink, horizontally placed in the test rig. Seven channels are carved in the aluminum block, each of them 35 mm long, 2 mm wide and 1 mm high (entailing an equivalent diameter of 1.33 mm), and two manifolds at the inlet and the outlet are provided in order to prevent flow maldistribution. The structure is sealed with an aluminum cogged cover and a rubber gasket. Four Pt100 cylindrical resistance thermometers are equidistantly placed along the channels for the measurement of the wall temperature. The actual distance between the RTDs placement and the channels wall is s = 2.5 mm. The heat is supplied from the bottom thanks to a slot carved in the aluminum main block, by means of AC power supply and a solid state relay which is able to give up to 400 V.

Two different heated lengths are used in this paper: in the first set of experiments, the heat is provided with a ceramic heater directly put in the slot underneath the test section. The heating element is able to supply up to 697 W (at 25 °C) over a base area of 2.50x2.50 cm^2.In this case, the heated length is L_h = 25 mm and the L_h/D ratio (with D the equivalent diameter of each minichannel) is equal to 18.75.

For the second set of experiments, the heat is provided with a cartridge ceramic heater, accommodated in a copper block, whose pyramidal edge is put in the slot underneath the aluminum test section. According to the manufacturer, the cartridge heater is able to provide up to 3000 W (at 600 °C and 400 V). In this case, the slot carved in the aluminum block has been modified in order to obtain a heated length equal to the channels length (L_h = 35 mm and L_h/D = 26.25). The copper block geometry has been chosen by simulating the temperature field with different dedicated software. The pyramidal shape allows to preserve the perpendicular direction of the heat flux in respect to the minichannels cross section.

The whole test rig is insulated with an appropriate layer of synthetic rubber, with a thermal conductivity less than 0.042 W/(m K) within the range of operating conditions investigated. Particular

attention has been paid to the test section: in the first set of experiments, the aluminum block has been covered with several layers of synthetic rubber, whilst in the case of the cartridge heater, a considerable amount of mineral wool (0.038 W/m K) has been used to cope with the higher temperatures of the copper block.

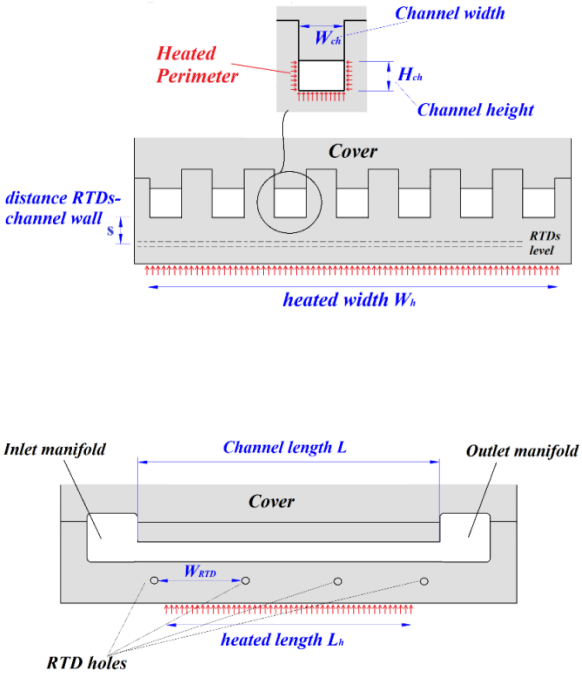
Both the L_h/D test section arrangements have been tested in liquid single phase in order to verify the correct insulation. The imposed heat has been compared to the heat absorbed by the sub-cooled liquid and the heat losses have been then calculated.

The adiabaticity tests for the first test section have shown that the heat losses could be considered negligible. In this case, the effective heat $\dot{Q}_{eff}$ has been considered equal to the electrical measurement.

The adiabaticity tests for the second test section arrangement (L_h/D = 26.25, with the presence of the copper block) have led to calculated heat losses approximately equal to 5-6 %, at any heat imposed. It was found that the heat losses were mainly dependent on the difference between the copper element temperature and the ambient temperature. Therefore, a simple equation for the evaluation of the heat losses has been implemented and used for the calculation of the effective heat:

$$\dot{Q}_{loss} = 1.478 \cdot \left(T_{copper} - T_{amb}\right)^{0.5706} \quad (1)$$

Fig. 2 displays a schematic picture of the test section with its geometrical characteristics. Fig. 3 shows the test section corresponding to the higher L_h/D ratio with the copper block exposed before the insulation process.



Feature	Value	Symbol
Number of channels	7	N
Channels width	2 mm	W_{ch}
Channels height	1 mm	H_{ch}
Channels length	35 mm	L
Equivalent diameter: $\frac{4 \cdot W_{ch} H_{ch}}{2 \cdot (W_{ch} + H_{ch})}$	1.33 mm	D
Heated width	25 mm	W_h
Heated lengths	25/35 mm	$L_{h,}$
Distance RTD-wall	2.5 mm	s
Distance between RTDs	10 mm	W_{RTD}

Figure 2. Geometrical details of the test section

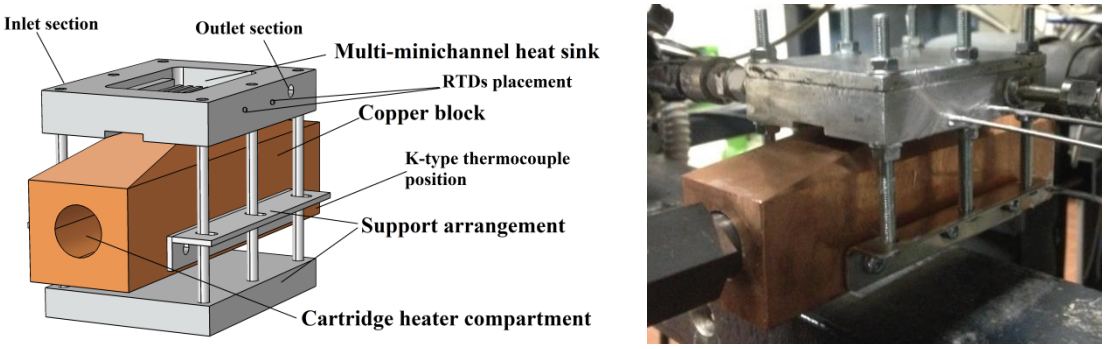


Figure 3. Schematic and real set-up of the test section with the copper block and the cartridge heater, corresponding to the highest L_h/D arrangement

2.3. Measurement uncertainties

The temperature measurements at the inlet and the outlet of the test section, as well as in the rest of the test rig, are obtained with 4-wire Pt100 resistance thermometers placed outside the pipe walls with a nano-aluminum thermal compound. According to the manufacturer, their maximum uncertainty should not exceed 0.180 °C. The four Pt100 cylindrical RTDs for the measurement of the wall temperature carry instead a lower overall uncertainty of 0.154 °C.

Two absolute pressure transducers (0-50 bar) measure the absolute pressure at the inlet of the test section and right before the liquid receiver. By taking into account the non-linearity and the repeatability effects, the resulting uncertainty is 0.3% of the read value.

The differential pressure transducer (0-60 kPa) gives a span error of 0.75% at full scale, resulting in an absolute uncertainty of 0.45 kPa.

The Coriolis mass flow meter has been calibrated up to the 2% of the full scale (2.3 g/s). The maximum uncertainty was found to be 1% of the measurement and this value is used for the whole range of our experiments.

The electrical power measurements have been taken with a digital wattmeter (0-4.00 kW), whose uncertainty is claimed to be 1% of the reading.

Thanks to the manufacturers information, the B type uncertainty has been composed with the standard deviation of the measured parameters in the recording time. Finally, the expanded uncertainty of the measured parameters has been evaluated by considering a coverage factor k = 2, thus guaranteeing a confidence level of 95%. The expanded uncertainty of all the derived parameters is then evaluated by means of the law of propagation of errors.

All the experiments carried-out for this paper present an uncertainty of the CHF inferior to 3 %. The operating parameters evaluated at the critical conditions in terms of mass velocity G and saturation temperature T_{sat} have an uncertainty always inferior to 16 % and 3.5 %, respectively. The higher uncertainty of the mass flux is due to fluctuations of the mass flow rate approaching the critical condition, thus resulting into a higher standard deviation.

3. Method

3.1. Experimental procedure

The purpose of each test is to describe a complete boiling curve from the onset of the boiling region up to the critical condition. All the boiling curves were therefore obtained in steady state conditions, meaning that the desired inlet pressure (i.e. saturation temperature), inlet sub-cooling and mass velocity were set and kept constant throughout the test procedure.

The system pressure was fixed by setting the desired temperature of the thermostatic bath, while the mass flow rate was obtained with a specific inverter frequency for the circulation pump.

Significant adjustments of the mass flow rate and system pressure could be achieved by manually turning the main loop by-pass valve.

Small alterations of the inlet temperature and therefore of the inlet sub-cooling were possible with the aid of the sub-cooler by-pass circuit.

Once all the desired parameters were fixed, for both the test sections the heat was supplied in small increments by changing the voltage applied to the ceramic elements within the range 0-230 V.

All the parameters were monitored and controlled with Labview software and Arduino One controller.

As regards the first test section, the heater temperature was constantly monitored with a K-type thermocouple integrated into the heater itself and the power supply was automatically shut off when it reached the limit of 120 °C not to irreparably damage the test section. The integrity of the second test section was instead ensured by two K-type thermocouples inserted in the copper structure. In this case, the power supply was expected to be cut off in case the copper block reached the threshold of 300 °C.

The system was considered stabilized when the relative uncertainty of the main parameters such as the mass flux, saturation temperature and heat imposed were inferior to 10%, 2% and 3%, respectively, in the recording time of 2 minutes with a recording frequency of 1 Hz. For each point of the boiling curve, the nominal value was assigned to the sample average value.

The following data reduction process was implemented in MATLAB software [12], while the calculation of all the thermodynamic properties was carried out with the software REFPROP 9.0, developed by Nist [13].

3.2. Data reduction

The mass flux inside the test section is evaluated from the measured mass flow rate:

$$G = \frac{\dot{m}}{W_{ch} \cdot H_{ch} \cdot N} \tag{2}$$

where N, W_{ch} and H_{ch} are the number of minichannels, the channels width and height, respectively, and $\dot{m}$ is the measured mass flow rate.

The inlet saturation temperature and enthalpy are evaluated with the inlet temperature and the inlet pressure and the aid of the software REFPROP 9.0. [13].

The actual wall temperature is calculated by considering 1-D heat conduction inside the aluminum test section. A preliminary analysis with dedicated calculation software has in fact confirmed that the axial conduction in the aluminum block is negligible if compared to the main flux in the vertical direction.

$$T_{w,i} = T_{RTD,i} - \frac{\dot{q}_b \cdot s}{k_{al}} \tag{3}$$

In the above equation, $T_{RTD,i}$ is the measured temperature of the i^{th} thermocouple, k_{al} is the aluminum thermal conductivity (fixed at 240 W/m K) and $\dot{q}_b$ is the base heat flux, evaluated as the ratio of the effective heat power (see equation (1)) over the base heated area, which is 2.50x2.50 cm^2 and 2.50x3.50 cm^2 for the first and the second test section, respectively.

The actual wall heat flux is instead evaluated with the same procedure used by Park and Thome [14], by considering the heated perimeter and a fin efficiency η.

$$\dot{q}_w = \frac{\dot{Q}_{eff}}{N \cdot L_h \cdot (W_{ch} + 2H_{ch} \cdot \eta)} \tag{4}$$

The value of the fin efficiency is firstly guessed equal to 0.90, then it is evaluated with an iterative procedure until it reaches a fixed value, according to the following equations [15], in which the HTC is the mean heat transfer coefficient obtained at the highest wall superheat and W_{fin} is the fin width:

$$\eta = \frac{\tanh(m \cdot H_{ch})}{m \cdot H_{ch}} \tag{5}$$

$$m^2 = \frac{HTC \cdot 2(W_{fin}+L_h)}{k_{al} \cdot W_{fin} \cdot L_h} \tag{6}$$

$$HTC = \frac{\dot{q}_w}{\Delta T_{w,max}} \tag{7}$$

The outlet enthalpy and quality are finally obtained with an energy balance on the test section. The outlet pressure is calculated by subtracting the pressure drop from the inlet pressure value.

$$h_{out} = h_{in} + \frac{\dot{Q}_{eff}}{\dot{m}} \tag{8}$$

3.3. CHF detection method

The critical condition usually refers to the point of the boiling curve in which a sharp rise of the wall superheat is detected without significant increment of the imposed heat flux. In this case, the liquid phase in contact with the heated wall is replaced by the vapor, which is not able to handle the thermal load due to its lower heat transfer efficiency.

In case of multi-minichannel systems, other researchers [14]-[16]-[17] have found that the sharp rise of the wall temperature is instead substituted by a gentler change in the boiling curves slope. This behavior is probably due to the heat redistribution aided by conduction phenomena, which is more evident when increasing the thickness of the solid substrate and/or the number of minichannels [18]. Furthermore, the mass velocity also has a mitigating effect on the critical condition [14]-[19].

Fig. 4 displays four different experimental boiling curves taken with R134a at T_{sat} = 45 °C with two different mass velocities and with the two L_h/D available. The wall superheat on the x-axis is the maximum value among the four RTDs placed along the channels. Fig. 4(a) refers to the minimum mass flux investigated of 150 kg/m^{2}s, while Fig. 4(b) refers to the maximum mass flux tested of 350 kg/m^{2}s. In both figures, the shape of the curves significantly changes with L_h/D, indicating an effect of the solid copper substrate. The change in the boiling curve slope is also more abrupt in the first case of G = 150 kg/m^{2}s, confirming the effect of the mass velocity on the critical values.

There is therefore the need to identify an objective method to detect the CHF condition. Following the same approach of Mauro et al. [16], the critical heat flux has been defined as the heat flux in which the boiling curve decreases its slope below a chosen threshold of 1.0 W/cm^2 K.

Pragmatically, the slope of the boiling curve presents an irregular trend and it is not always monotonically decreasing. The search of CHF begins only when the slope (evaluated with spline interpolation from the experimental data) is always below a threshold value of 1.5 W/cm^2 K. Fig. 5 depicts the slope of the boiling curve obtained with refrigerant R134a at T_{sat} = 65 °C and G = 300 kg/m^2 s. The CHF research begins from the green line, in which the slope is always inferior to the threshold of 1.5 W/cm^2 K. The actual CHF is found when the curve first reaches the imposed threshold of 1.0 W/cm^2 K. This point is displayed with a red star in the diagram in Fig. 5. Either in case this method does not find the CHF or the critical wall superheat is higher than 25 K, the CHF value is conventionally defined as the wall heat flux corresponding to a wall superheat of 25 K.

In this procedure, the overall CHF uncertainty should take into account the uncertainty related to the boiling curve slope, which is affected by the wall superheat excursion. However, since the CHF phenomenon is obtained with sharp increases of the wall temperature for small heat flux variations, the

uncertainty of the measured temperature is not of primary importance and the CHF overall uncertainty has been calculated by only taking into account the electrical measurement.

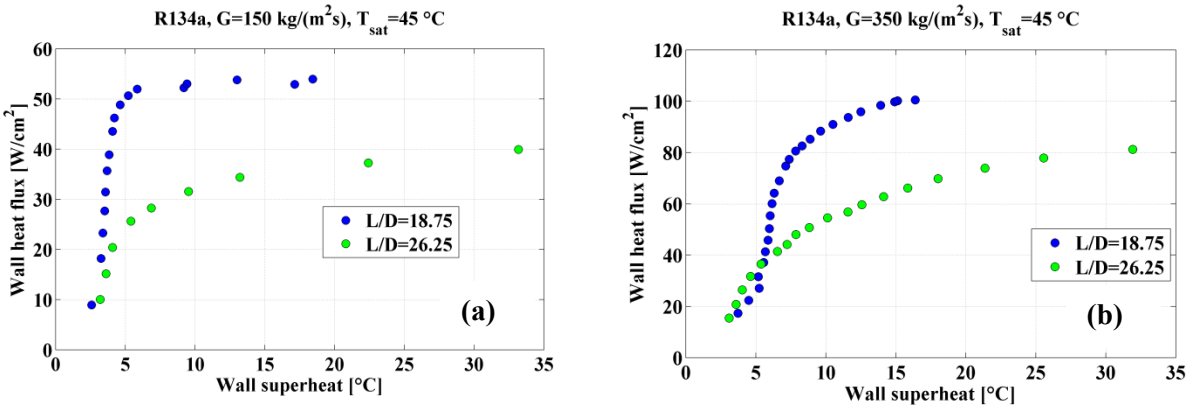


Figure 4. Boiling curves obtained with refrigerant R134a at T_{sat} = 45 °C. Effect of L_h/D ratio at: (a) G = 150 kg/m^2 s and (b) G = 350 kg/m^2 s.

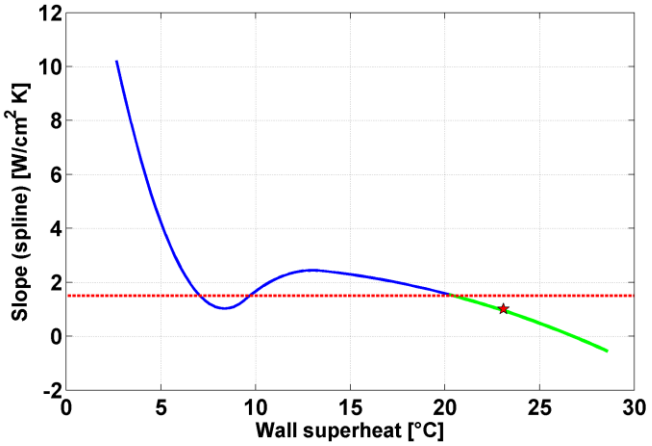


Figure 5. CHF detection method applied to R134a at G = 300 kg/m^2 s and T_{sat} = 65 °C. The red dashed line identifies the search threshold of 1.5 W/cm^2 K, and the actual CHF value is obtained at a slope of 1.0 W/cm^2 K, highlighted with the red star

4. Experimental results

The main CHF tests have been performed with refrigerant R134a and its low-GWP substitute R1234yf, within a saturation temperature range of 25-65 °C and a mass flux range of 150-350 kg/m^2 s. Each test has been repeated for two different L_h/D ratios of 18.75 and 26.25, respectively. The effect of all these parameters on both fluids is exposed in Fig. 6(a)-(b), in which the experimental CHFs and their expanded uncertainty are displayed against the saturation temperature. Each marker and color refer to different mass velocities and the two different L_h/D ratio values are highlighted with solid and dashed line styles.

It is quite evident that the effect of the saturation temperature on the detected critical heat fluxes is almost negligible. Regarding refrigerant R134a (Fig. 6(a)), the CHF values remain nearly the same regardless the mass flux or the L_h/D ratio. The highest decrement is recorded for G = 300 kg/m^2 s and L_h/D = 26.25, with the CHF passing from 71.9 to 62.3 W/cm^2 when the saturation temperature rises from 25 to 65 °C. For refrigerant R1234yf (Fig. 6(b)), the CHF values remain nearly the same at any mass flux for the lowest L_h/D ratio = 18.75, whereas the descending trend is more evident for the highest L_h/D ratio of 26.25: at G = 352 kg/m^2 s, the CHF reduces of approximately 20% (from 71.0 to 56.6 W/cm^2) at increasing saturation temperature.

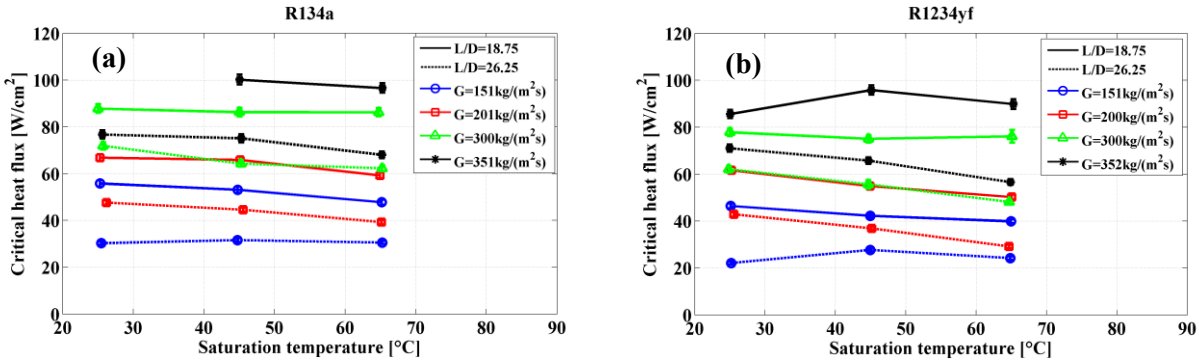


Figure 6. Experimental CHF values with their expanded uncertainty band as a function of the saturation temperature. Each color and marker are referred to a particular mass velocity. The solid and dashed lines refer to L_h/D ratios of 18.75 and 26.25, respectively. The examined fluids are: (a) R134a and (b) R1234yf.

The parametric effect of the working fluid, the L_h/D ratio and the mass flux is depicted in Fig. 7, in which the experimental CHF values with their expanded uncertainty have been plotted versus the mass velocity, for both fluids and L_h/D ratios investigated. The saturation temperature has been instead fixed to 65 °C.As expected, the mass flux has a great effect on the critical values, since CHF increases significantly (up to 130%) passing from 150 to 350 kg/m^2 s, assuming almost a linear trend, for both fluids and L_h/D ratios tested.

Between the two fluids, R134a shows better cooling performances than R1234yf: at the same conditions, the CHF for the new low-GWP fluid is roughly the 20% lower than that of R134a.

A different L_h/D ratio obtained by changing the heated length L_h in the two test sections used leads to significantly different CHF values. For both refrigerants, at L_h/D = 26.25 the CHF results are lower and the gap is larger for higher mass velocities. Similar results have been obtained in other works available in open literature [7]-[10]-[11]. Specifically, for refrigerant R134a, at G = 150 kg/m^2 s, CHF passes from 47.0 to 31.0 W/cm^2, while at G = 350 kg/m^2 s, it goes from 91.0 to 58.0 W/cm^2, with a reduction of 36%. For refrigerant R1234yf, at G = 150 kg/m^2 s CHF passes from 40.5 to 22.0 W/cm^2, while at G = 350 kg/m^2 s, it goes from 90.2 to 58.0 W/cm^2, with a reduction of 36 % as well. Similar trends are observed for different saturation temperatures.

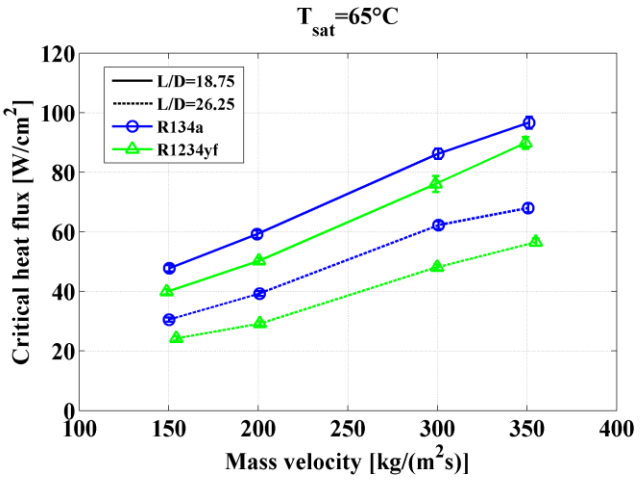


Figure 7. Experimental CHF values with their expanded uncertainty band as a function of the mass velocity for refrigerants R134a and R1234yf with two different L_h/D ratios of 18.75 and 26.25. The diagram refers to a saturation temperature of 65 °C.

5. Conclusions

The saturated critical heat flux (CHF) in a multi-minichannel heat sink at different operating conditions has been studied in this paper. The effect of the mass velocity, saturation temperature and working fluid has been first investigated. Two test section set-up arrangements have been structured in order to achieve two different heated lengths and therefore two different L_h/D ratios. The effect of this parameter has also been studied.

The experimental results have shown that R134a has better cooling performances that those of its substitute R1234yf, with a CHF from 10 to 20 % higher when evaluated at the same thermodynamic conditions.

The effect of the saturation temperature is almost negligible for both fluids and all the mass velocities, but it is amplified in case of the highest L_h/D ratio of 26.25, for which the CHF reduction is roughly the 20 % when passing from 25 to 65 °C

CHF increases linearly with mass velocity, regardless the fluid used and the saturation temperature. The trends do not change with the two different L_h/D ratios.

The heated length has a strong influence on the experimental CHF results. By increasing the L_h/D ratio, the CHF significantly reduces of about 35 % for both fluids in all the operating conditions tested. Slightly greater differences are found for higher mass velocities.

Although the obtained results are in agreement with other works available in open literature, the effect of the L_h/D ratio has still to be fully clarified in the available correlations and further research with new L_h/D ratios, fluids and thermodynamic conditions would be of use to increase the experimental database.

References

[1] United States Semiconductor Industry Association (SIA), European Semiconductor Industry Association (ESIA), The Japan Electronics and Information Technology Industries Association (JEITA), The Korean Semiconductor Industry Association (KSIA), The Taiwan Semiconductor Industry Association (TSIA) 2009 *Int Technol Roadmap Semicond*. http://www.itrs.net/Links

[2] Mudawar I2001 Assessment of high-heat-flux thermal management schemes. *IEEE Trans Compon Packag Technol* **24** 122-141

[3] Royne A, Dey CJ and Mills DR 2005 Cooling of photovoltaic cells under concentrated illumination: a critical review. *Solar Energy Materials and Solar Cells* **84** 451-483

[4] Palm B 2001 Heat transfer in microchannels *Microscale Thermophys Eng* **5** 155-175

[5] Bergles AE and Kandlikar SG 2005 On the nature of critical heat flux in microchannels *J Heat Transf* **127** 101-107

[6] Ribatski G 2013 A critical overview on the recent literature concerning flow boiling and two-phase flows inside micro-scale channels *Experimental heat transfer: a Journal of thermal energy generation, transport, storage, and conversion* **26:2-3** 198-246

[7] Tanaka F, Hibiki T and Mishima K 2009 Correlation for flow boilingcritical heat flux in thin rectangular channels *Journal of heat transfer* **131** 121003-7

[8] Saha S K and Celata G P 2016 Instability in flow boiling in microchannels *Springer briefs in applied science and technology, Thermal engineering and applied science* **8884** DOI 10.1007/978-3-319-23431-1

[9] Boyd R D 1985 Subcooled flow boiling critical heat flux (CHF) and its application to fusion energy components. Part II: a review of micro-convective, experimental and correlation aspects *Fusion Technology* **7** 31-52

[10] Wu Z and Li W 2011 A new predictive tool for saturated critical heat fluxin micro/mini-channels: effect of the heated length-to-diameter ratio International Journal of Heat and Mass Transfer **54** 2880-2889

[11] Wojtan L, Revellin R and Thome J R 2006 Investigation of saturated critical heat flux in a

single, uniformly heated microchannel *Experimental Thermal and Fluid Science* **30** 765-774.
[12] MATLAB release. *Natick, Massachussets, United States, The MathWorks, Inc.*
[13] Lemmon E W, Mc Linden M O and Huber M L 2009 REFPROP *NIST Standard Reference Database* **23***, Version 9.0*
[14] Park J E and Thome J R 2010 Critical heat flux in multi-microchannel copper elements with low pressure refrigerants *Int. J. of Heat and Mass Transfer* **53** 110-122
[15] Baehr HD and Stephan K 2006 Heat and mass transfer *Springer 2nd edition*
[16] Mauro A W and Thome J R, Toto D and Vanoli G P 2010 Saturated critical heat flux in a multi-microchannel heat sink fed by a split flow system *Experimental Thermal and Fluid Science* **34** 81-92
[17] Koşar A and Peles Y 2006 Critical heat flux of R-123 in silicon-based microchannels. *Journal of Heat Transfer* **129** 844-851
[18] Saenen T and Thome J R 2016 Dynamic numerical microchannel evaporator model to investigate parallel channel instabilities *Journal of Electronic Packaging* **138** 010901-13
[19] Mastrullo R, Mauro A W, Thome J R, Vanoli G P and Viscito L 2016 Critical heat flux: performance of R1234yf, R1234ze and R134a in an aluminum multi-minichannel heat sink at high saturation temperatures *Int. J. Thermal Sciences* **106** 1-17